GA–A26576

THE GENERAL ATOMICS FUSION THEORY PROGRAM REPORT FOR GRANT YEAR 2009

by
PROJECT STAFF

OCTOBER 2009

DISCLAIMER

GA–A26576

THE GENERAL ATOMICS FUSION THEORY PROGRAM REPORT FOR GRANT YEAR 2009

by
PROJECT STAFF

Work supported by
the U.S. Department of Energy
under Grant No. DE-FG03-95ER54309

GENERAL ATOMICS PROJECT 03726
OCTOBER 2009

ABSTRACT

The objective of the fusion theory program at General Atomics (GA) is to significantly advance our scientific understanding of the physics of fusion plasmas and to support the DIII–D and other tokamak experiments as well as ITER research activities. The program plan is aimed at contributing significantly to the Fusion Energy Science, the Tokamak Concept Improvement, and ITER goals of the Office of Fusion Energy Sciences (OFES). Significant progress was made in each of the important areas of our research program during the last grant year GY09. This includes extensive testing of the pedestal height model EPED1 against a large number of H-mode discharges from various tokamaks under different plasma operating conditions, demonstration using the 3D MHD code NIMROD that in DIII-D discharges rapidly cooled by massive Ar injection the escaping electrons striking the outer divertor early in time and the main vacuum chamber later in time consistent with the experiments, development of a new TGLF collision model that demonstrates much better agreement against a large database of collisional GYRO simulations than the previous model, development of the TGYRO (steady state gyrokinetic transport) code that was successful in doing direct GYRO simulations of a DIII-D discharge with energy transport flows balanced against source flows, and performance of ORBIT-RF/AORSA simulations of DIII-D and NSTX HHFW experiments that qualitatively reproduces an outward radial shift of the fast-ion spatial distribution as measured by the FIDA diagnostic. GA theory staff also participated and contributed to the ReNew process.

TABLE OF CONTENTS

1. HIGHLIGHTS OF THEORY WORK IN GY09

During the past grant year, significant progress was made in each of the important areas of our research program:

- Extensive testing of the pedestal height model EPED1 including accurate predictions of the pedestal height and width for a series of DIII-D and JET discharges with ρ_* varied more than a factor of 4.
- Demonstration using the ELITE code that there can be significant advantages of the snowflake configuration for peeling-ballooning stability.
- Demonstration using the MARS-F code that the ideal plasma response to external perturbation fields depends strongly on the arrangement of the external perturbing fields.
- Demonstration using the 3D MHD code NIMROD that in DIII-D discharges rapidly cooled by massive Ar injection the escaping electrons striking the outer divertor early in time and the main chamber later in time consistent with the experiments.
- Demonstration using NIMROD simulations with fixed and ramped RMP fields that the same final unstable mode amplitudes are achieved in both cases but residual oscillations from initial transients persist in the fixed field case.
- Performance of M3D-C1 simulations of model DIII-D and NSTX ohmic discharges that indicates localized particle sources may lead to core toroidal rotation the direction of which depends on the location of the source.
- Development of a new eigenvalue solver within GYRO that confirms the characteristics of the leading unstable energetic-particle driven toroidal Alfvén eigenmode and explicitly shows coexistence of multiple high-frequency instabilities.
- Performance of large nonlinear GYRO simulations of energetic particle (EP) turbulence that clearly shows the transition from pure ITG/TEM to EP driven turbulence as the EP drive strength is increased.
- Demonstration that GYRO can simulate a very high β DIII-D discharge and gets past the subcritical β limit to about 90% of the ideal high-n limit with good confinement when the high experimental level of $E \times B$ shear is applied.
- Performance of a study of the Onsager symmetries of the flux-gradient relations for gyro-Landau fluid models that shows there are non-trivial constraints on the form of the equation closure that must be satisfied and points the way for a new TGLF version.
- Development of the TGYRO (steady state gyrokinetic transport) code that was successful in doing direct GYRO simulations of a DIII-D discharge with energy transport flows balanced against source flows.

- Development of a new TGLF collision model that demonstrates much better agreement against a large database of collisional GYRO simulations than the previous model.
- Development of a new TGLF saturation rule based on the geodesic acoustic mode (GAM) frequency that naturally gives the correct ratio of ETG to ITG electron thermal transport and provides a better fit to the low-k GYRO simulation database.
- Addition of calculation of the transport coefficients due to gyro-viscosity to the gyro-kinetic neoclassical transport code NEO and demonstration in a DIII-D momentum flux calculation that the gyro-viscous flux is comparable in magnitude to the neoclassical flux.
- Performance of comparative calculations between ORBIT-RF and AORSA that supports the validity of the Monte-Carlo heating model and the readiness of the iterative coupling between ORBIT-RF and AORSA for an improved modeling of ICRF experiments.
- Performance of ORBIT-RF/AORSA simulations of DIII-D and NSTX HHFW experiments that qualitatively reproduces an outward radial shift of the fast-ion spatial distribution as measured by the FIDA diagnostic.
- Development of a first theoretical penetration model for the formation of a pellet cluster stream when a super large, high-speed D_2 pellet is shattered by collision against a striker plate configuration.
- Demonstration in a new analytical calculation that the poloidal electric field contribution can increase the neoclassical toroidal angular momentum flux by the order of the square root of the aspect ratio.
- Development of an analytical description of tokamak single and double null divertor equilibrium using the homogeneous solution of the Grad-Shafranov equation together with a particular Solovev-like solution.
- Development of a new source code management utility to allow IMFIT to efficiently manage the latest F90/95 EFIT source for different devices and operating platforms.
- Implementation of the TGLF confinement model in the ONETWO transport code using the improved GCNMP solver with flow representation and verification of test results against the XPTOR transport code.

In addition, GA theory staff also participated and contributed to the ReNew process, as well as served on several panels.

As a consequence of these results, scientists from the Theory Group were selected to give a number of invited talks and colloquia as highlighted in the next section. Sections 3 through 6 provide more detailed descriptions of the advances and achievements made in each of the major areas.

2. SIGNIFICANT PRESENTATIONS IN GY09

2009 PRESENTATIONS

51th APS DPP meeting in Atlanta, Georgia November 2–6, 2009:

- E.M. Bass gives an invited presentation "Gyrokinetic Simulations of Enhanced Alpha Transport by Destabilized Alfven Turbulence."
- J. Candy gives an invited presentation "Predictive Gyrokinetic Transport Simulations and Application of Synthetic Diagnostics."
- M. Choi gives an invited presentation "Iterated Finite Orbit Monte Carlo Simulation with Full Wave Fields for Tokamak ICRF Wave Heating."
- A.D. Turnbull gives an invited presentation "A New View of Internal Kink Modes and their Relation to the Sawtooth Instability."

50th APS DPP meeting in Dallas, Texas November 17–21, 2008:

- E.A. Belli gave an invited presentation "Drift-Kinetic Simulations of Neoclassical Transport."
- P.B. Snyder gave an invited presentation "Development and Validation of a Predictive Model for the Pedestal Height."

22nd IAEA Fusion Energy Conference in Geneva, Switzerland October 13–18, 2008:

- C. Holland gave an oral presentation "Validation of Gyrokinetic Transport Simulations Using DIII-D Core Turbulence Measurements."
- V.A. Izzo gave a presentation "RMP Enhancement Transport and Rotation Screening in DIII-D Simulations."
- P.B. Snyder gave a presentation "Pedestal Stability Comparison and ITER Pedestal Prediction."
- G.M. Staebler gave a presentation "Testing the Trapped Gyro-Landau Fluid Transport Model with Data from Tokamaks and Spherical Tori."

Pedestal ITPA meeting in Milan, Italy October 20–22, 2008:

- P.B. Snyder gave a presentation "Development and Testing of the EPED1 Pedestal Model and Predictions for ITER."

SciDAC Winter School at UC-Irvine, California February, 25 2009:

- R. Waltz gave a lecture "Gyrokinetic Simulations and the GYRO Code."

US-Japan RF Workshop in Toba, Japan March 16–18, 2009:

- M. Choi gave a presentation "Comparison of Monte-Carlo Ion Cyclotron Heating Model with Full-Wave Linear Absorption Model."

Scientific Grand Challenges in Fusion Energy Sciences in Washington, DC March 19, 2009:

- J. Candy gave a presentation "Status of GYRO / NEO / TGYRO."

Extreme Computing Workshop in Gaithersburg, MD March 2009:

- P.B. Snyder gave a presentation "Challenges in the Physics of the Edge Barrier Region."

Transport Modeling / Integrated Operation Scenario ITPA meeting in Naka, Japan March 31 –April 2, 2009:

- G. Staebler gave a presentation "TGLF Modeling of DIII-D ITER Scenario Discharges."

Pedestal ITPA meeting in Cadarache, France April 20–22, 2009:

- P.B. Snyder gave two presentations "Progress and Plans for the EPED1 Model and Comparison to Experiment" and "Discussion of Work Plan for ITER Urgent Issue in Pedestal Structure."

Joint EU-US Transport Task Force Workshop in San Diego, California April 28 – May 1, 2009:

- E.M. Bass gave a presentation "Gyrokinetic Simulation of Energetic Particle Transport."
- P.B. Snyder gave a presentation "Development and Validation of a Pedestal Model for the Pedestal Height EPED1."
- J.E. Kinsey gave a presentation "Gyrokinetic Simulation Test of Quasilinear and Tracer Transport."

4th IAEA-TM Meeting on the Theory of Plasma Instabilities in Kyoto, Japan May 18–20, 2009:

- E.M. Bass gave a presentation "Gyrokinetic Simulation of Energetic Particle Transport."

1st Integrated Modeling Expert Group Annual Meeting in ITER Headquarters Cadarache, France June 23–26, 2009:

- L.L. Lao gave a presentation "Interpretive and Data Processing – IMFIT and Magnetic Reconstruction and Stability."

18th Topical Conference on RF Power in Plasma in Gent, Belgium June 24–26, 2009:

- M. Choi gave a presentation "Simulation of the DIII-D Beam Ion Heating Experiment Using a Monte-Carlo Particle Code Combined with a Full Wave Code."

Turbulent Mixing and Beyond International Conference in Trieste, Italy July 27 – Aug 7, 2009:

- R. Waltz gave an invited lecture "Gyrokinetic Simulation of Turbulent Transport in Fusion Plasmas."

3. ADVANCES IN MHD EQUILIBRIUM AND STABILITY RESEARCH

3.1. EQUILIBRIUM RECONSTRUCTION AND ANALYTICAL DIVERTOR EQUILIBRIUM

EFIT F90/95 Development: A new unified F90/95 version of EFIT for different operating platforms has been developed and tested. All grid-size related arrays have been modified to allow dynamic memory allocation so that a single EFIT version can be used for different grid sizes. A summer intern student carried out the work.

Analytical Tokamak Divertor Equilibrium: An analytical description of tokamak single and double null divertor equilibrium has been constructed using the homogeneous part of the exact solution of the Grad-Shafranov equation together with a particular Solovev-like solution.

3D Perturbed MHD Equilibria: Several approaches to compute 3D perturbed MHD equilibria have been investigated. These include the analytic expansion method used by Zwingmann to study the toroidal field ripple effects on 2D axisymmetric equilibrium in TORE-SUPRA with EFIT, as well as the free-energy perturbation approach used by NMA to study RWM stability. The Zwingmann's approach is expected to be valid in the regime of high n (of the order of aspect ratio) and with weak coupling to plasma (assuming the plasma response is weaker than the vacuum field). For lower n an alternative method is needed. The free-energy perturbation approach can be applied without using the virtual casing principle by making changes to the DCON and VACUUM code.

3.2. EDGE STABILITY AND EPED1 PEDESTAL HEIGHT MODEL VALIDATION

EPED1 Validation: The EPED1 predictive model for the pedestal height and width has been successfully applied to a large set of discharges on the DIII-D, JET, and JT-60U tokamaks. The ratio of predicted to observed pedestal height was 1.02 ± 0.13 for a series of discharges on all three tokamaks (21 DIII-D, 16 JT-60U, 4 JET), as shown in Fig. 1. Observed trends with triangularity, current, magnetic field, collisionality and Shafranov shift (global β) were correctly predicted by the model. The DIII-D discharges studied include a dedicated experiment in which EPED1 predictions were made before the experiment, and a set of ITER-demonstration discharges. These results were presented as an invited talk at the 2008 APS/DPP meeting.

The pedestal height in the JT-60U discharges has long been observed to vary with time over the length of the discharges. Studies with EPED1 find that these changes in pedestal height with time can be attributed to changes in the Shafranov shift (due to changing global β) which impacts peeling-ballooning stability, and to changes in pedestal collisionality, which alters the edge bootstrap current and also affects peeling-ballooning stability.

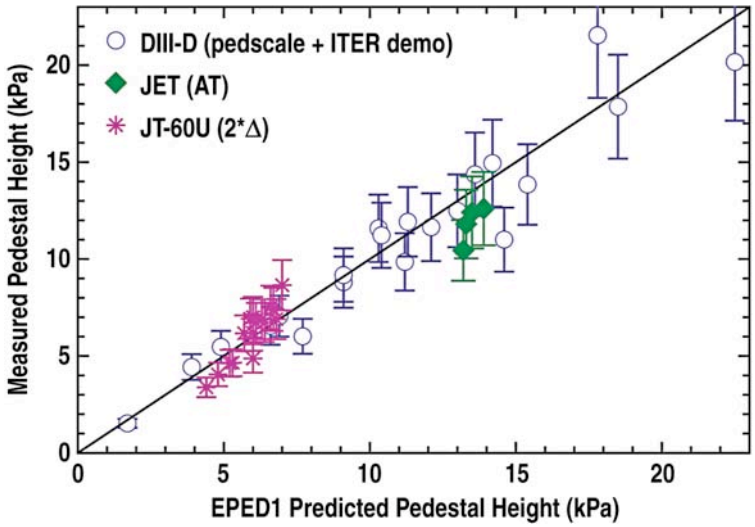

Fig. 1. A new predictive model of the pedestal height, EPED1, was used to make pedestal height predictions for 21 DIII-D discharges, 4 JET discharges, and 16 JT-60U discharges. Comparison between EPED1 predicted and observed pedestal height in these experiments is shown, with an overall ratio of predicted to observed pedestal height of 1.03±0.12.

Extensive statistical studies of the DIII-D pedestal database find a good correlation of the DIII-D pedestal width with 0.076 times the square root of pedestal poloidal β. Once this dependence is taken into account, the correlation with other dimensionless parameters is weak. Both results are consistent with qualitative predictions from kinetic ballooning mode theory.

The EPED1 model was also tested on a pair of DIII-D discharges in which ECH power was substituted for neutral beam power, to test the impact of heating source on plasma performance. EPED1 predictions were found to be in good agreement with the observed pedestal height, both with pure NBI heating and with NBI plus ECH.

ELITE was also used to study edge stability on NSTX, in cases where ELMs were triggered by magnetic perturbations. The studies find that the NSTX discharges are becoming more unstable shortly before ELMs are observed.

Lastly, the EPED1 model was tested on a series of discharges on DIII-D and JET in which the normalized gyro-radius (ρ_*) was varied more than a factor of 4 while other key dimensionless quantities were held approximately fixed. The EPED1 predictions of the pedestal height and width were found to be accurate in both DIII-D and JET. EPED1 predicts little or no dependence of the pedestal width on ρ_*, in agreement with the experimental results.

ITER Edge Stability Modeling: The dependence of the predicted pedestal height on density for both a baseline and an advanced operational regime were studied. The EPED1

predicted pedestal height, in terms of normalized beta at the top of the pedestal, is similar in the baseline and AT regimes, and increases with density (or equivalently, Greenwald fraction), in both cases, from a value of $\beta_{Nped} \approx 0.55$ at low density up to a value of $\beta_{Nped} \approx 0.70$ at high Greenwald fraction.

A study of the edge stability of the snowflake configuration was also performed and found that there could be significant advantages of the configuration for peeling-ballooning stability.

3.3. MARS-F PLASMA RESPONSE TO EXTERNAL PERTURBATION FIELDS

MARS-F Ideal Plasma Response: In the limit in which the plasma is assumed to behave as a vacuum, the response to external resonant perturbing non-axisymmetric magnetic fields from MARS-F has been shown to have excellent agreement with that computed previously by SURFMN, a Biot-Savart code with realistic coil arrangements. In this comparison, both SURFMN and MARS-F are also shown to agree with an analytic model for the fields produced by the external coils. With the agreement in the vacuum response, MARS-F was then used to compute the plasma response in the ideal plasma limit. The 2D MHD response computed by MARS-F showed that the net ideal plasma plus vacuum response depends strongly on the arrangement of the external perturbing fields.

MARS-F Resistive Plasma Response: The effect of plasma resistivity on plasma response to perturbation magnetic field imposed by an external source has been studied for a rotating plasma with a separatrix. It is found that on the non-resonant helicity side, the plasma response is not much affected by plasma resistivity. On the resonant side, the overall plasma response is generally suppressed by the shielding effect caused by internal resonances. Even with resistivity and partial reconnection, the reconnection level is much lower than the full vacuum response. Thus we expect that field line stochasticity is much more reduced than that obtained with the assumption of vacuum response

3.4. NIMROD AND M3D-C1 SIMULATIONS AND DEVELOPMENT

NIMROD RMP Field Ramp: The implementation of time-varying externally applied error fields has been tested in NIMROD through a direct comparison between two cases run with fixed amplitude RMP fields and the identical cases with time varying boundary condition to model the I-coil current ramp beginning at $t=0$ and achieving the same final amplitude. For these low S simulations, the RMP ramp time of 0.1 ms is comparable to a reconnection time, and the RMP fields are held fixed at their peak amplitude for several more reconnection times as a steady state solution is achieved. One pair of simulations has no plasma rotation, and thus no RMP screening, and should achieve the same steady state regardless of initial conditions.

In the fixed amplitude case, the plasma responds violently to the superimposed vacuum fields at $t=0$, and even as a steady state is approached, a small residual $n=1$ oscillation

continues (Fig. 2). In contrast, the identical case with the RMP field ramp obtains identical final amplitudes for the $n=3$ and $n=1$ field components, but does not exhibit the $n=1$ oscillation. Two cases with toroidal plasma rotation are also compared, and also achieve very similar steady state solutions, including a large amplitude $n=1$ oscillation associated with the plasma rotation. Although hysteresis is possible in a rotating case, it is not expected in the highly resistive and viscous regime of the simulations. In the future, hysteresis effects will be explored in a higher rotation or lower resistivity regime.

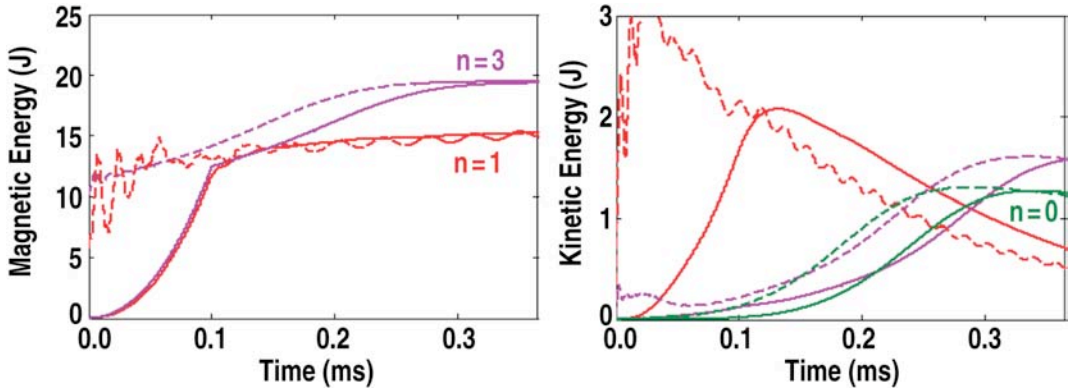

Fig. 2. Evolution of magnetic and kinetic energy in the $n=0$, 1, and 3 modes for NIMROD RMP simulations with fixed amplitude RMP (dashed lines) imposed at $t=0$ and with a linear I-coil ramp from $t=0-0.1$ ms. The same final amplitudes are achieved in both scenarios, but residual oscillations from initial transients persist in the fixed field case.

DIII-D Disruption and Runaway Electron Modeling: Several simulations of DIII-D discharges rapidly cooled by massive Ar injection were preformed with NIMROD to compare with Ar pellet injection experiments. These simulations made use of the newly developed runaway electron (RE) orbit following model in NIMROD to examine RE confinement during the disruption. Additionally, $n=3$ perturbing fields associated with the DIII-D I-coils were applied in some cases, to determine if RMP fields can help to de-confine runaways. In the NIMROD results, both even and odd parity I-coil fields actually enhance RE confinement relative to the case with no applied $n=3$ fields. The $n=3$ fields have no direct impact on the runaway confinement time, but indirectly interact with the unstable modes responsible for the MHD crash early in the disruption. With $n=3$ fields present (in either parity) the MHD crash was dominated by an $m=1/n=1$ mode and a central region of good confinement remained throughout the evolution. The case with no perturbing fields was dominated by an $n=2$ mode and nearly all flux surfaces were destroyed, allowing REs in the core to quickly escape.

The simulations show the escaping electrons striking the outer divertor early in time, and the main chamber later in time, which appears consistent with the experiments. The NIMROD radiated power spike at the time of the MHD onset has quantitative similarity to the radiated power spike in DIII-D, and the total radiated energy during the disruption shows

a very close match between simulation and experiment. The effects of the $n=3$ fields may contradict preliminary DIII-D results, and needs to be further explored.

M3D-C1 Development and Simulations: Several significant enhancements to M3D-C1, a resistive two-fluid code being developed in collaboration with PPPL and RPI, have been implemented. First, a capability for non-axisymmetric linear stability calculations has been implemented, which will allow accurate calculations of stability with resistive, two-fluid, and gyroviscous effects self-consistently included. Ballooning-mode benchmarks with ELITE have shown good agreement in the ideal limit. Second, the capability for non-rectangular simulation domains has been implemented, which is necessary for physics studies in which the boundary conditions may play an important role (such as resistive wall modes). Third, M3D-C1 may now be initialized with both EFIT and GATO equilibria. This will greatly facilitate the comparison of M3D-C1 results with those of experiments and other codes.

M3D-C1 has also been used to obtain accurate axisymmetric steady-states of model ohmic discharges in DIII-D and NSTX geometry. These steady-states are obtained by evolving the dynamical equations from an initial ideal-MHD equilibrium until the steady-state is reached (on transport time scales). The obtained solutions self-consistently include fluid velocity, resistivity, parallel- and gyro-viscosity, and particle and energy transport. It has been found that localized particle sources may lead to core toroidal rotation, the direction of which depends on the location of the source.

M3D-C1 Benchmarking Calculations: Benchmarking of M3D-C1 calculations of the linear stability of ELMs in the ideal limit is nearing completion. The calculation of growth rates in diverted geometries in the ideal limit has proven to be challenging due to the high-resolution requirements and the sensitivity of the growth rate, especially at high toroidal mode numbers. Good agreement is found at low and intermediate toroidal mode numbers. Once benchmarking in the ideal case is complete, M3D-C1 will be used to calculate stability with Spitzer resistivity profiles, two-fluid effects, and FLR effects included; this should reveal self-consistent ω_* stabilization and resistive ballooning modes.

Improvements to the method used by M3D-C1 to calculate fields from non-axisymmetric coil sets have now brought vacuum calculations into excellent agreement with those of SURFMN and MARS. Calculations including plasma response are underway. M3D-C1 has the advantages over MARS that it can calculate the dynamical response, as well as the response at the x-point of diverted plasmas.

3.5. SAWTOOTH STABILITY ANALYSIS

From additional equilibrium and stability analysis, the MHD burst in the DIII-D bean and oval sawtooth comparison experiments was found to correspond to the loss of the second $q=1$ surface formed after the crash in both discharges. Also, the sawtooth precursor, which is seen only for the oval discharge, appears definitely to be the ideal quasi-interchange helical

distortion, whereas the successor oscillations in the bean appear to be related to the subsequent island. The results continue to be consistent with the Wesson picture where the reconnection for the quasi-interchange occurs slowly through the sawtooth ramp phase but for the bean, the unstable standard internal kink reconnects rapidly during the crash.

A re-analysis of the results from numerical experiments in which the profiles from the bean and the oval taken from midway through the ramp were interchanged found a more complicated picture than previously thought. Using the new poloidal mode displacement criterion for distinguishing the quasi-interchange from the internal kink, the oval case with the bean profiles actually showed a quasi-interchange, suggesting it is the shape and not the profiles that determine the mode. However, this is contrary to the fact that the stability calculations for the ramp time sequence show that the bean actually does exhibit a quasi-interchange right after the crash. A possible resolution of this is that while the profiles are the prime determinant of the mode structure, the cross section modifies the transition point in q where the change in structure occurs. Taking profiles from the bean just before the crash instead of midway through the ramp may reproduce the internal kink in the oval. But this remains to be determined.

3.6. PORTING OF NOVA-K TO GA

A new interface between EFIT and NOVA-K using the GATO mapping as a stand-alone code was completed and tested for a DIII-D equilibrium. The test used an equilibrium recalculated by the PPPL q solver for discharge 96043 in order to compare the result directly with that using the built-in NOVA mapping, which can only accept q-solver equilibria. The equilibrium was unstable to an ideal internal kink mode. All quantities required by NOVA were compared by hand and found to check out to within 5% to 10%. The final eigenvalues from NOVA using the mapped input from GATO agreed with that from the built-in NOVA mapping to within a few percent. This should greatly expand the utility of NOVA and NOVA-K since the GATO mapping can equally well accept direct equilibria from EFIT and inverse equilibria from TOQ, TEQ, and JSOLVER. In addition, the GATO mapping has the capability of mapping arbitrarily close to a diverted surface, provision for up-down asymmetry, and has considerable flexibility in options for packing the mesh at particular surfaces.

An interface for transferring the radial fast ion pressure profile from ORBIT-RF to GATO and translation of this and the MHD equilibrium profiles to toroidal flux for subsequent passing to the NOVA-K code was completed. Coding was initiated to translate ORBIT-RF energy and pitch angle statistics into a distribution function for fitting to the NOVA-K model distribution.

4. ADVANCES IN TRANSPORT RESEARCH

4.1. GYRO APPLICATIONS AND IMPROVEMENTS

GYRO Simulation of the Subcritical β Limit: As previously reported, the 2005 β scan on Cyclone base and GA standard cases with the GYRO code was not able to operate past about half the ideal MHD critical β limit. In the past year considerable effort has been made to operate above what appears to be a *nonlinear subcritical MHD β limit*. The high-n ideal β limit is defined as the point where the growth rate extrapolated to the lowest possible wave number is greater than zero. The subcritical point for Cyclone is about 0.5 the ideal limit ($\beta_e^{crit}=1.5\%$) and may be induced by the increased effective pressure gradients from the nonlinearly driven zonal flows.

GYRO is able to operate with good numerical stability at very high transport levels above the subcritical point where steady and well defined saturated states may not exist. Neither the GS2 nor GEM has exceeded this subcritical limit although GENE has reported some mixed success with numerically unstable saturated states. The remedy appears to be the addition of $E\times B$ shear sufficient to reduce the transport at lower β by about half. The very high β DIII-D discharge 113333 manages to get past the usually lower external kink β limit to about 90% of the ideal high-n limit with good confinement. GYRO simulations of this discharge reasonably match the low transport only when the high experimental level of $E\times B$ shear is applied.

GYRO Angular Momentum Transport Corrections: More than 60 GYRO simulations had to be repeated to correct a GYRO code error. The correction was rather minor: the $E\times B$ shear pinch of angular momentum is somewhat weaker. An errata will be published soon. In addition, the GYRO formulation of toroidal angular momentum transport starting with a parallel velocity shifted Maxwellian has been compared to more formal theories from papers in the mid-90s. The differences due to neglect of perpendicular fluid rotation compared to parallel rotation (in pure toroidal rotation) appear to make about a 10% difference in the Coriolis drift. The more precise formulation is being added to GYRO (while keeping the previous) to quantify any small difference.

Momentum-Conserving Gyrokinetic Collision Operator: The effects of the momentum-restoring collisional dynamics on gyro-kinetic micro-turbulence have been studied with GYRO. The GYRO collision operator, which consists of a Lorentz operator for electrons and a Lorentz operator plus a simple momentum-restoring term for ion-ion collisions, has been upgraded to the Connor model. The split-operator collision step is implemented using the Peaceman-Rachford ADI algorithm, which is second-order accurate in time. Comparing a collision model consisting only of the Lorentz term with the new model which also includes the momentum-restoring term, little difference was found for a typical

linear ITG instability, as well as for the collisional zonal flow damping and the nonlinear ITG turbulence.

GYRO/TGLF Toroidal Angular Momentum (TAM) Transport Pinches and Residual Stress: TGLF has had the Kelvin-Helmhotz (main TAM transport) drive and Coriolis pinch in place for sometime. However, the $E\times B$ shear pinch needed to model the low-spontaneous toroidal rotation and no-rotation residual stress experiments has been a long-standing challenge. To model the correct $E\times B$ shear driven quasi-linear momentum transport, the $E\times B$ shear parameter must be removed from the nonlinear saturation rule (modeling the $E\times B$ shear quench) and put into the linear TGLF modes to break the symmetry about the $q=0$ mid-plane without invalidating the quench. We have now found a simple way to model this $E\times B$ shear symmetry breaking. Note both the Kelvin-Helmhotz (main TAM transport) drive and Coriolis pinch drive independently (and separately) break the symmetry required for TAM transport, but only the $E\times B$ shear symmetry breaking controls the residual stress which can be easily measured in DIII-D experiment at vanishing toroidal rotation. The latter will be a key focus of future TGLF momentum transport modeling. Numerous GYRO simulations to accurately find the $E\times B$ shear null TAM flow point have been done to provide simulation data for the TGLF model $E\times B$ shear pinch fit.

Gyrokinetic-Driven Field-Line Stochasticity: Field-line mapping codes have been developed to create Poincare plots of flux-surfaces in the presence of electromagnetic turbulence. The results indicate that even for β values where the gyro-kinetic simulations behave normally, the field lines can be almost completely stochastic.

GYRO Improvements: The physics of strong rotation in GYRO has been completely re-derived and re-implemented. The new formulation is consistent with that in NEO. The new code is now undergoing beta-testing.

A suite of tools for managing general geometry data with GYRO/NEO/TGYRO has been updated. The mapping from the equilibrium EQDSK data file is now handled by a tool derived from the GATO code geometry backend. The mapping to a model (Miller) or general shape is still handled by the new high-accuracy tool "FLUXFIT". This can be applied to cases which are based on ONETWO analysis (i.e., cases for which an ITERDB file is available) or cases for which a Plasma State file is available.

Steady-State Gyrokinetic Transport Development and Simulations: TGYRO development continues to move forward. Most recently we are focusing on details of the TGYRO iteration scheme. Simulations of DIII-D shot 101391 using TGYRO work very well except near the magnetic axis, for which the neoclassical transport is nearly zero, and turbulent transport vanishes. An interface to GYRO for use with both TGYRO and FMCFM has been developed.

4.2. GYRO ENERGETIC PARTICLE SIMULATIONS

GYRO Eigenvalue Solver: A linear eigenvalue solver built with PETSc and SLEPc libraries has been incorporated into GYRO. Performance characteristics for the new utility show substantial dependence on operational platform. Acceptable efficiency has been found on the NERSC Jacquard system. Linear, flux-tube simulations are underway to identify sub-dominant modes (EPM, BAE, etc.) predicted to exist when a hot, sparse species (such as fusion α particles) is present. The new utility will also help to definitively identify the onset of MHD instability when the pressure gradient comes entirely from the hot species, where growth rate and frequency of the dominant toroidal Alfvén eigenmode (TAE) have been mapped out using initial value simulations. The TAE growth rate exceeds that of the kinetic ballooning mode (KBM), even at very low $k_\theta \rho_s$, and beyond the MHD stability limit. The eigenvalue solver is being used to map the growth rate of the subdominant KBM as a function of $k_\theta \rho_s$ and hot species density gradient to verify the MHD stability threshold found from detailed flux-tube studies running in initial value mode without energetic particles.

GYRO Energetic-Particle Driven Turbulence: A number of large non-linear GYRO simulations of energetic particle (EP) turbulence have been run with the goal of solidifying understanding of TAE/EPM turbulence, particularly its onset as kinetic drive strength increases. Previous 16-mode, saturated cases including EP Alfvén drive have been extended to larger 40-mode simulations. Saturation behavior is a bit better in the larger simulations, so background ITG/TEM drive was not lowered below the GA standard case level as previously planned. A range of EP drive strengths (expressed through the density of energetic particles n_{EP}) has been run, clearly showing the transition from a pure ITG/TEM spectrum (where EPs act as tracer particles) to cases where the EPs drive TAE/EPM turbulence (Fig. 3). Saturated states are still impossible to find above n_{EP} = 0.8%, not far above the TAE/EPM linear threshold of n_{EP} = 0.5%, when background shear is not included. Forty mode simulations including $E \times B$ drift shear can saturate at higher drive levels, but identifying a shearing rate that still shows TAE/EPM drive has proved difficult. A shearing rate of γ_E = 0.03 shows some promise, but more time is required to get reliable statistics on the turbulent fluctuations for these cases. A DPP invited paper on this material is in preparation.

4.3. TGLF TRANSPORT MODEL DEVELOPMENT AND VALIDATION

TGLF Development: A study of Onsager symmetries of the flux-gradient relations for gyro-Landau fluid (GLF) models shows that there are non-trivial constraints on the form of the closure of the GLF equations for both the slab and toroidal limits that must be satisfied in order to preserve the Onsager symmetries. Including electromagnetic fluctuations generates additional constraints. Symmetries between various terms in flux-gradient relations are known to ensure the positivity of entropy production. These Onsager symmetries in collisional transport theory result from terms having the same energy moments of the

distribution function and the theory of gyrokinetic turbulence driven fluxes yields similar symmetries. The analysis shows that if these symmetries are not respected in the closure of the GLF equations then the ratio of ion to electron energy flux or of energy flux to particle flux will be inaccurate even if the linear growth rates are accurate. This points the way for a future version of TGLF.

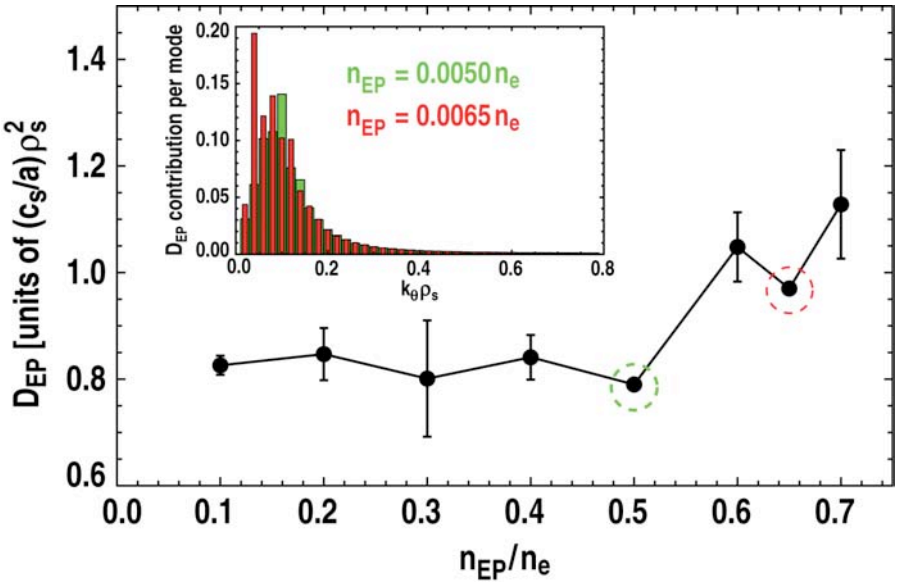

Fig. 3. Energetic particle density diffusion coefficient D_{EP} showing increase with the onset of low-n TAE/EPM turbulence.

Rotation was added to TGLF. The parallel velocity shear and Coriolis terms were straightforward to add to the TGLF equations. The $E\times B$ velocity shear was also added to the TGLF eigenmode solution by a generalization of the successful "quench rule". The quench rule subtracts the $E\times B$ velocity shear from the linear growth rate with a constant multiplier determined from the best fit to the GYRO simulations. This quench rule does not break the mode parity along the magnetic field and hence cannot reproduce the viscous stress due to $E\times B$ velocity shear. The new generalized quench rule includes a model for the radial wave number induced by the $E\times B$ velocity shear. The radial model number breaks the mode parity and the coefficients of the model for the radial mode number are fit to give the best fit to the GYRO viscous stress. This simple model obtains a good fit for the standard case. Other cases are being run with GYRO to test the parametric variation of the model coefficients. The TGLF eigenmode solution method does not need to be modified in order to include all of these rotation terms. Ironically, an elegant rigorous method to transform the rest frame gyrokinetic equations into a rotating frame where the electric field and its shear vanish did not succeed in reproducing the GYRO non-linear results with $E\times B$ velocity shear. The transformation method gave eigenvalues that were stabilized by the $E\times B$ velocity shear but not in the same way as observed in GYRO. For example the high-k modes were stabilized first rather than the lowest-k modes as seen in GYRO. It is unclear what is "wrong" with the

transformation method but it did not resolve the radial mode structure. The generalized quench rule uses a model for the radial mode structure. Based on the agreement with GYRO this must be critical.

A new saturation rule has been developed for TGLF. It was inspired by the work by Holland and Waltz showing that the saturation level of the turbulence depends on the geodesic acoustic mode (GAM) frequency. The new model eliminates one fit parameter compared to the previous model. It uses the acoustic mode frequency instead of the curvature drift frequency in the formula. The new rule has one less parameter than the previous model. It naturally gives the correct ratio of ETG to ITG electron thermal transport and fits the low-k GYRO simulation database better than the previous rule.

TGLF Verification and Validation: Work has continued on testing a new collision model in TGLF and comparing the predicted diffusivities against nonlinear GYRO runs including both collisions and Miller geometry. Recent comparisons between TGLF and GYRO show that the new TGLF model demonstrates much better agreement against a database of 53 nonlinear collisional GYRO simulations with Miller geometry. The average RMS errors in the (χ_i, χ_e) decreased substantially from (21%, 26%) to (10%, 13%). This is shown in Fig. 4.

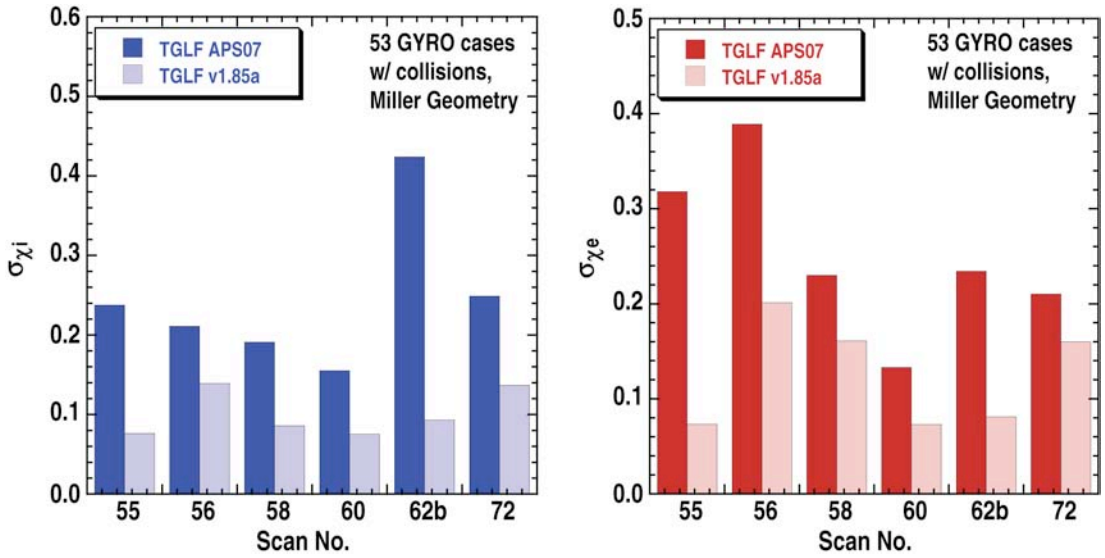

Fig. 4. RMS errors for the ion (blue) and electron (red) energy diffusivities computed between TGLF with the new (v1.85a) and old (APS07) collision models and GYRO for 53 collisional cases with Miller geometry.

A few attempts at applying TGLF within the H-mode pedestal region have also been performed. Using a high resolution transport analysis of DIII-D H-mode 98889, TGLF was successful in predicting the energy transport with the boundary conditions extended out to a radius of $\rho = 0.99$. While the predicted T_e profile is somewhat too high near the top of the pedestal, the model was successful in predicting the formation of an H-mode pedestal.

Analysis of the diffusivities show that the ion channel is mildly turbulent and the ETG modes contribute to roughly half of the electron energy transport.

TGLF Release: The TGLF linear stability and quasi-linear transport code is now available for public distribution. The package includes a stand-alone driver for computing linear drift wave eigenmodes or quasi-linear fluxes. The TGLF model has been extensively verified against fully gyrokinetic linear stability calculations and non-linear turbulence simulations using the GYRO code. The TGLF model has proven to be a more accurate model of the gyrokinetic results than its widely used predecessor GLF23. As reported at the 2007 APS conference, the TGLF model predicts the core temperature profiles for a database of more than 100 discharges from three tokamaks with greater accuracy than GLF23. After filling in a user agreement form, a copy of the TGLF source code can be downloaded from its webpage.

4.4. NEOCLASSICAL TRANSPORT AND FLOW

Neoclassical Flows in the Pedestal: NEO has been used to analyze the impurity poloidal flow in the H-mode edge for a typical C-Mod plasma. The simulations were done with three species: deuterium ions, electrons, and boron impurities. We find large differences in the magnitude of the computed and measured poloidal flows in the core, even accounting for the relatively large error in the measurements due to the fact that CXRS is a low signal measurement. In the pedestal, we find that the results are closer, suggesting that the flows are in fact essentially neoclassically driven there, although NEO predicts a more narrow pedestal width. By solving the higher-order drift-kinetic equations, we find that the finite-orbit-width effects are negligible even in the steep-gradient region and thus cannot account for the differences. Other effects, such as orbit loss, will be explored in future work.

Neoclassical Gyro-Viscous Fluxes: The calculation of the transport coefficients due to gyro-viscosity was added to NEO for use in transport calculations, such as TGYRO. The gyro-viscous fluxes are determined by the second-order gyrophase-dependent component of the distribution function. The gyro-viscous particle and energy fluxes are non-zero only with both up-down asymmetric flux-surface shape and strong rotation effects, while non-zero gyro-viscous momentum flux requires only up-down asymmetry. For typical DIII-D plasmas, we find that the gyro-viscous particle and energy fluxes are negligible compared to the neoclassical fluxes. However, it is important that the gyro-viscous particle flux not be neglected in transport calculations, as it is the sum of the gyro-viscous and neoclassical particle fluxes which is ambipolar, rather than the neoclassical fluxes themselves. For the momentum flux, we find that the gyro-viscous flux for the primary ion species and electrons in DIII-D is comparable in magnitude to the neoclassical flux, though both are expected to be small compared with the turbulent momentum flux.

Neoclassical Angular Momentum Transport: A complete expression was obtained for the poloidal variation of the electrostatic potential in the banana regime for large aspect ratio

flux surfaces using the method of matched asymptotic expansions. The result exhibits a finite discontinuity at the innermost point of a flux surface instead of a divergence as previously reported. Using this expression in combination with the solution of the linearized drift kinetic equation with a model collision operator, the part of the toroidal angular momentum flux due to the poloidal electric field is calculated. The result is larger than the one in existing works, which neglect the poloidal electric field, by the order of the square root of the aspect ratio.

5. ADVANCES IN RF HEATING AND FUELING RESEARCH

5.1. ORBIT-RF DEVELOPMENT AND MODELING

ICRF Monte-Carlo Heating Model Testing: To fully account for the wave-particle interaction physics in ion-cyclotron resonant frequency (ICRF) heating experiment, finite orbit effects and non-Maxwellian distribution have to be self-consistently coupled with full-wave solutions. For this purpose, the 5D Monte-Carlo code ORBIT-RF is being coupled with the 2-D full wave code AORSA to iteratively evolve the ion distribution in x-v phase space that is used to update the dielectric tensor in AORSA for evaluating the full-wave fields. It is demonstrated that using the full-wave fields from a Maxwellian dielectric tensor in AORSA and confining the resonant ions to their initial orbits in ORBIT-RF, ORBIT-RF largely reproduces the AORSA linear wave absorption profiles for fundamental and higher harmonic ICRF heating. An exception is an observed inward shift of the ORBIT-RF absorption peak for high harmonics near the magnetic-axis compared with that of AORSA, which can be attributed to a finite orbit width effect with more refined model of the wave-particle interaction time. The success of this verification supports the validity of the Monte-Carlo wave-particle interaction model and the readiness of the iterative coupling between ORBIT-RF and AORSA for an improved modeling of ICRF heating experiments.

ORBIT-RF Development: ORBIT-RF has been improved to use the beam-ion distribution function from the PTRANSP NUBEAM module. NUBEAM calculates fast-ion distribution averaged in each bin of energy, pitch, and space. To use PTRANSP distribution function as an initial condition, an option to convert the bin averaged distribution function to the particle distribution has been implemented in ORBIT-RF. To verify the consistency of PTRANSP bin-averaged distribution function with the converted Monte Carlo particle distribution, a comparison between the EFIT experimentally reconstructed beam-ion pressure profile and the calculated one from ORBIT-RF has been performed. The result indicates reasonably good agreement. This particle distribution function is passed to AORSA to calculate the fast wave fields. Simulations of beam-ion interaction with fast wave in DIII-D experiments using ORBIT-RF coupled with AORSA are underway.

ORBIT-RF Modeling of DIII-D and NSTX Fast-Wave Experiments: The ORBIT-RF/AORSA ICRF package is being applied to analyze DIII-D and NSTX high harmonic fast-wave heating experiments. With ICRF on, ORBIT-RF/AORSA simulations qualitatively reproduce an outward radial shift of the fast-ion spatial distribution due to finite drift-orbit motion as measured by the DIII-D and NSTX FIDA diagnostic, although the shift appears to be more radially outward than indicated by the FIDA measurements.

5.2. DISRUPTION MITIGATION

Modeling of DIII-D Low-Z Pellet Ablation Experiment: A discharge (134317) from the DIII-D low-Z pellet ablation experiment was analyzed using the electron temperature cooling model recently put forth by P. Parks. In this discharge, a small ~ 2 mm diameter polystyrene shell pellet, filled with argon gas by permeation, was injected into the plasma. The sublimation energy of the polystyrene monomer C_8H_8 is 113 kJ/mole. This is equivalent to 0.021 eV expended per electron ablated. This relatively small value suggests that ablation rate can be calculated by using the standard ablation model (SAM) for mono-atomic/diatomic cryogenic pellets where the sublimation energy is negligibly small. We used the SAM assuming the monomer behaves like a big atom with atomic weight 104, with the ablation rate formula pre-multiplied by the constant numerical coefficient 0.62 that came from fitting the penetration prediction with the actual measured penetration distance in the DIII-D plasma recorded from camera images of the visible light emission from the ablation plume.

The predicted T_e profile after pellet cooling is compared with the original T_e profile. There is considerable disagreement between the predicted and the measured T_e profiles. The temperature dip in the measure profile is much deeper. One possible reason for the discrepancy is that the cooling model was done for irrational surfaces only. Cooling on rational surface with shorter connection lengths will be stronger as the volume of the plasma energy reservoir is less. The other possibility is that the cooling of the plasma triggers enhanced radiation cooling from in situ impurities. Both of these ideas will be explored in future work.

Penetration Model: The first theoretical model of the penetration for a pellet cluster stream formed when a super large, high-speed D_2 pellet is shattered by collision against a striker plate configuration was developed. Injection of such a spray of pellet fragments is being investigated as a new method of quenching avalanche runaways during fast plasma terminations. The model assumes that all pellets are same size and uniformly distributed in the stream, which is assumed to have the shape of a long cylinder of specified dimensions. The two coupled differential equations describing the penetration and ablation of the stream into the plasma were cast in dimensionless form using only a single independent variable formed by the combination of the rescaled time and space variables. The solutions will be applied to the recent experiment carried out on DIII-D.

6. ADVANCES IN INTEGRATED MODELING

6.1. IMFIT DEVELOPMENT AND PLASMA STATE FILE

IMFIT Development: Several recommendations suggested by the IMFIT Advisory Committee that met last September at GA have been implemented into IMFIT. These include replacing the existing CVS based IMFIT repository using the SVN Subversion Control System and improving the IMFIT Framework to enable embedding of native Python coding inside the Task-Flow file for error control and branching. Many other improvements to the Equilibrium, Transport, and stability GUIs have also been made including a GUI to perform kinetic EFIT reconstruction. A global data module was also added in order to facilitate the passing of common information among the various physics components (e.g., working directory).

Various improvements were also made to IMFIT to enhance its portability and usability. An EFIT source-code management system under IMFIT was developed and tested to improve EFIT portability. A dynamic linking capability was added to IMFIT in order to facilitate customization and portability. The ONETWO GUI was significantly updated. IMFIT can now automatically choose the appropriate code executable based on certain system-level parameters (e.g., CPU and OS). Users can also modify their IMFIT preferences and request technical support from within the main GUI. Work to prepare a first version of IMFIT for public testing is underway and nearly completed.

IMFIT Plasma State File: As part of the PTRANSP and IMFIT projects, a standardized set of variables, sufficient to translate to and from a set of application codes, is under development using the self-describing NetCDF data format. An important and substantial part of both projects is the development of suitable interfaces for user-transparent communication between PTRANSP, GCNMP, ONETWO, and XPTOR, as well as other codes in the future. A summer intern student made a significant contribution to this effort by creating cross-reference maps of the quantities involved.

6.2. ONETWO TRANSPORT CODE DEVELOPMENT

TGLF Implementation and Testing: A version of the TGLF confinement model has been installed and operational in the ONETWO transport code based on the GCNMP global Newton solver. To deal with extremely computationally intensive models such as TGLF, several improvements to GCNMP have been made. These include a Jacobian-free solution method, finite-difference form of the transport equations in terms of fluxes rather than diffusivities, and a “compact derivative” scheme that uses all grid points to define higher-order derivatives across the entire computational grid simultaneously. Compact derivatives provide a smoother representation of derivatives compared to the standard finite representation method.

Benchmarking calculations against the XPTOR transport code have also been carried out for two DIII-D discharges and a FDF configuration. ONETWO/GCNMP results with TGLF agree with those from XPTOR and the experimentally measured profiles to within 10% to 15% difference (Fig. 5). Some of this difference may be due to the difference in the background neoclassical confinement models used in these two codes. As shown in Fig. 5, the predicted temperature profiles from GCNMP are smoother when the compact derivative approach is used in the analysis.

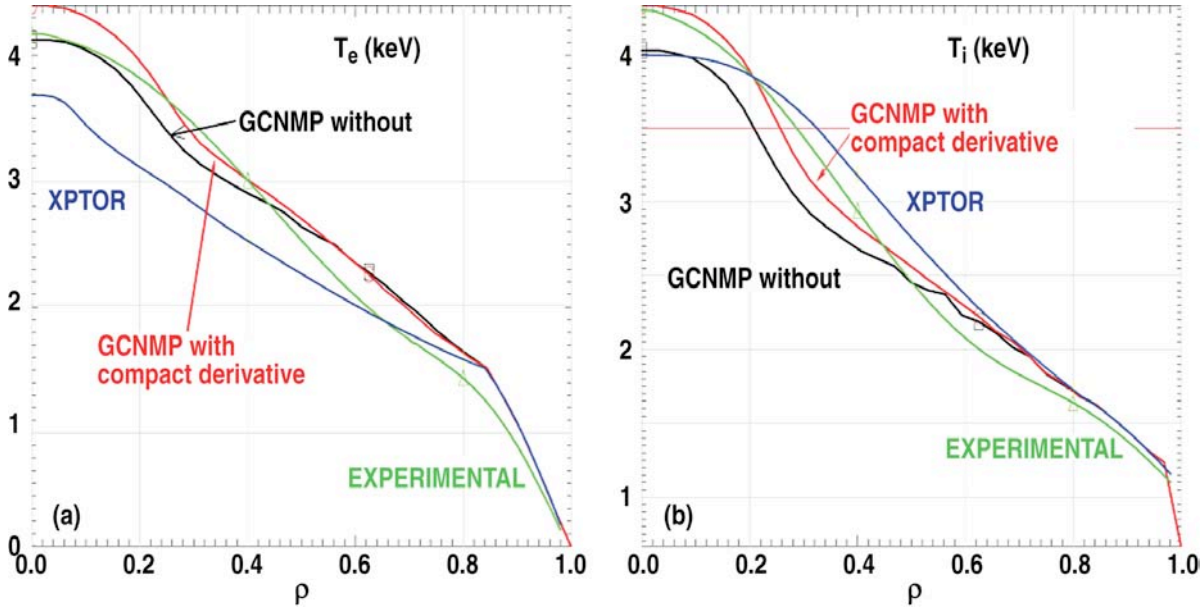

Fig. 5. Comparison of electron (a) and ion (b) temperature profiles computed using ONETWO/GCNMP and the TGLF transport model with (red) and without (black) compact derivatives applied against those from XPTOR (blue) and experimental measurements (green) for DIII-D discharge 131711.

7. PUBLICATIONS

PRIMARY THEORY AUTHORS FOR 2009

C. Angioni, J. Candy, E. Fable, M. Maslov, A.G. Peeters, R.E. Waltz, and H. Weisen, "Particle Pinch and Collisionality in Gyrokinetic Simulations of Tokamak Plasma Turbulence," Phys. Plasmas **16**, 060702 (2009).

E.A. Belli and J. Candy, "An Eulerian Method for Solution of the Multispecies Drift-Kinetic Equation," Plasmas Phys. Control. Fusion **51**, 075018 (2009).

S. Braun, P. Helander, E.A. Belli, and J. Candy, "Effects of Impurities on Collisional Zonal-Flow Damping in Tokamaks," Plasmas Phys. Control. Fusion **51**, 065011 (2009).

J. Breslau, N.M. Ferraro and S.C. Jardin, "Some Properties of the M3D-C1 Form of the 3D Magnetohydrodynamics Equations," Phys. Plasmas **16**, 092503 (2009).

J. Candy, C. Holland, R.E. Waltz, M.R. Fahey, and E. Belli, "Tokamak Profile Prediction Using Direct Gyrokinetic and Neoclassical Simulation," Phys. Plasmas **16**, 060704 (2009).

J. Candy, "A Unified Method for Operator Evaluation in Local Grad-Shafranov Plasma Equilibria," Plasmas Phys. Control. Fusion **51**, 105009 (2009).

A. Castali, T. Gerbaud, P. Hennequin, C. Bourdelle, J. Candy, F. Clariet, X. Garbet, V. Grandgirard, O.D. Gurcan, S. Heuraux, G.T. Hoang, C. Honore, F. Imbeaux, R. Sabot, Y. Sarazin, L. Vermare, and R.E. Waltz, "Turbulence in the TORE SUPRA Tokamak: Measurements and Validation of Non-linear Simulations," Phys. Rev. Lett. **102**, 165005 (2009).

A. Casati, T C. Bourdelle, X. Garbet, F. Imbeaux, J. Candy, F. Clairet, G. Dif-Pradalier, G. Falchetto, T. Gerbaud, V. Grandgirard, O.D. Gurcan, P. Hennequin, J. Kinsey, M. Ottaviani, R. Sabot, Y. Sarazin, L. Vermare, and R.E. Waltz, "Validating a Quasi-Linear Transport Model versus Nonlinear Simulations," Nucl. Fusion **49**, 085012 (2009).

M. Choi, V.S. Chan, L.A. Berry, E.F. Jaeger, D. Green, P. Bonoli, J. Wright, and RF SciDAC Team, "Comparison of Monte-Carlo Ion Cyclotron Heating Model with Full-Wave Linear Absorption Model," Phys. Plasmas **16**, 052513 (2009).

M.S. Chu and M. Okabayashi, "Stabilization of the External Kink and Resistive Wall Mode," submitted to Plasmas Phys. Control. Fusion, 2009.

N.M. Ferraro and S.C. Jardin, "Calculations of Two-Fluid Magnetohydrodynamic Axisymmetric Steady-States," J. Comp. Phys. **228**, 7742 (2009).

N.M. Ferraro, S.C. Jardin, and X. Luo, "Boundary Conditions with Reduced Quintic Finite Elements," submitted to J. Comp. Phys., 2009.

J.R. Gary, J. Candy, J. Cobb, R.H. Cohen, T. Epperly, D.J. Estep, S. Krasheninnikov, A.D. Malony, D.C. McCune, L. McInnes, A. Pankin, S. Balay, J.A. Carlsson, M.R. Fahey, R.J. Groebner, A.H. Hakim, S.E. Kruger, M. Miah, A. Pletzer, S. Shasharina, S. Vadlamani, D. Wade-Stein, T.D. Rognlien, A. Morris, S. Shende, G.W. Hammett, S. Indireshkumar, A. Yu Pigarov, and H. Zhang, "Concurrent, Parallet, Multiphysics Coupling in the FACETS Project," J. Phys.: Conf. Ser. **180**, 012056 (2009).

J.D. Hanson, S.P. Hirshman, S.F. Knowlton, L.L. Lao, E.A. Lazarus, and J.M. Shields, "V3FIT: a Code for Three-Dimensional Equilibrium Reconstruction," Nucl. Fusion **49**, 075031 (2009).

C. Holland, A.E. White, G.R. McKee, M.W. Schafer, J. Candy, R.E. Waltz, L. Schmitz, and G.R. Tynan, "Implementation and Application of Two Synthetic Diagnostics for Validating Simulations of Core Tokamak Turbulence," Phys. Plasmas **16**, 052301 (2009).

V.A. Izzo, P.B. Parks, and L.L. Lao, "DIII-D and ITER Rapid Shutdown with Radially Uniform Deuterium Delivery," Plasmas Phys. Control. Fusion **51**, 105004 (2009).

J.E. Kinsey, G.M. Staebler, and R.E. Waltz "TGLF Transport Modeling of DIII-D Hybrid Discharges," in preparation for submission to Phys. Plasmas, 2009.

L. Lin, M. Porkolab, E.M. Edlund, M. Greenwald, N. Tsujii, J. Candy, R.E. Waltz, and D.R. Mikkelsen, "Studies of Turbulence and Transport in Alcator C-Mod Ohmic Plasmas with Phase Contrast Imaging and Comparison with gyro-kinetic Simulations," Plasmas Phys. Control. Fusion **51**, 065006 (2009).

C. I. Pusztai, T. Fulop, J. Candy, and R.J. Hastie, "Collisional Model of Quasilinear Transport Driven by Toroidal Electrostatic Ion Temperature Gradient Modes," Phys. Plasmas **16**, 072305 (2009).

J.P. Qian, L.L. Lao, Q.L. Ren, H. Rinderknecht, F. Volpe, C. Zhang, and B.N. Wan. "Equilibrium Reconstruction of Plasma Profiles Based on Soft X-Ray Imaging in DIII-D," Nucl. Fusion **49**, 025003 (2009).

J. Qian, B. Wan, L.L. Lao , S. Biao, S.A. Sabbagh, Y. Sun, D. Liu, B. Xiao, Q. Ren, X. Gong, and J. Li, "Equilibrium Reconstruction in EAST Tokamak," Plasma Sci. Technol. **11**, 142 (2009).

J. Qian, B. Wan, S. Biao, L.L. Lao, B. Xiao, J. Li, S. Lin, and Z. Luo, "Observational of Poloidal Current Flowed to the Vessel after Failure of Vertical Position feedback Control in EAST Tokamak," Chinese Phys. B **18**, 1172 (2009).

Q. Ren, M.S. Chu, L.L. Lao, H. St. John, R. La Haye, Y.M. Jeon, Z. Cheng, D. Zhou, G. Li, J.M. Park, and J. deGrassie, "Momentum Transport in DIII-D Discharges with and without Magnetohydrodynamic (MHD) Activity," Plasma Sci. Technol. **11**, 127 (2009).

Y. Shen, J. Dong, H. He, and A.D. Turnbull, "Preliminary Study of Ideal Operational MHD Beta Limit in HL-2A Tokamak Plasmas," Plasma Sci. Technol. **11**, 131 (2009).

P.B. Snyder, R.J. Groebner, A.W. Leonard, T.H. Osborne, and H.R. Wilson, "Development and Validation of a Predictive Model for the Pedestal Height," Phys. Plasmas **16**, 056118 (2009).

P.B. Snyder, N. Aiba, M. Beurskens, R.J. Groebner, L.D. Horton, A.E. Hubbard, J.W. Hughes, G.T.A. Huysmans, Y. Kamada, A. Kirk, C. Konz, A.W. Leonard, J. Lönnroth, C.F. Maggi, R. Maingi, T.H. Osborne, N. Oyama, A. Pankin, S. Saarelma, G. Saibene, J.L. Terry, H. Urano, and H.R. Wilson "Pedestal Stability Comparison and ITER Pedestal Prediction," Nucl. Fusion **49**, 085035 (2009).

R. Srinivasan, L.L. Lao, and M.S. Chu, "Analytical Description of Tokamak Equilibrium with Divertor Configuration," submitted to Plasmas Phys. Control. Fusion, 2009.

R.E. Waltz and C. Holland, "Numerical Experiments on the Drift Wave - Zonal Flow Paradigm for Nonlinear Saturation," Phys. Plasmas **15**, 122503 (2008).

R.E. Waltz, A. Casati, and G. Staebler, "Gyrokinetic Simulation Test of Quasilinear and Tracer Transport," Phys. Plasmas **16**, 072303 (2009).

ACKNOWLEDGMENT

This work supported by the U.S. Department of Energy under Grant No. DE-FG03-95ER54309.